Characterization of the chemical composition of uranium microparticles with irregular shapes using standardless electron probe microanalysis and micro-Raman spectrometry

Mouad Essani, Emmanuelle Brackx, Fabien Pointurier, Faustine Berthy, Emmanuel Excoffier, Philippe Jonnard

Characterization of the chemical composition of uranium microparticles with irregular shapes using standardless electron probe microanalysis and micro-Raman spectrometry

Mouad Essani[1,3,*], Emmanuelle Brackx[1], Fabien Pointurier[2], Faustine Berthy[2], Emmanuel Excoffier[1], Philippe Jonnard[3]

[1]CEA, DEN, DMRC, Univ Montpellier, F-30200 Marcoule, France

[2]CEA, DAM, DIF, F-91927 Arpajon, France

[3]Sorbonne Université, CNRS UMR 7614, Laboratoire de Chimie Physique- Matière et Rayonnement, 4 place Jussieu, F-75252 Paris Cedex 05, France

ABSTRACT: We describe an approach enabling the identification of the elemental composition of uranium microparticles with undefined geometry using standardless quantitative Electron Probe MicroAnalysis (EPMA) and Micro-Raman Spectrometry (MRS). The standardless procedure is based on a ZAF peak-to-background quantitative method in combination with Monte Carlo simulations. The experimental X-ray spectra were measured with an energy dispersive spectrometer attached to a scanning electron microscope. In order to account for the X-ray intensity loss due to the transmission of electrons in microparticles with irregular shapes, a method was developed enabling the determination of an apparent thickness of the particle by means of the mean distance that electrons travel inside the particle before being transmitted. Size effects were further taken into account by using peak-to-background ratios and performing simulations on a particle with a thickness equal to the apparent thickness. In order, to assess the validity of the standardless procedure in EPMA, weight fractions were determined for NIST homogeneous spherical microparticles of K411 glass and compared to certified ones. The correction of size effects was achieved and lead to accurate quantitative results with absolute relative deviations less than 9%. The model used for the determination of the apparent thickness was validated on the set of spherical K411 particles and enabled to conduct quantifications on irregularly shaped uranium microparticles. The chemical composition of uranium particles was further investigated using MRS which enabled to verify the reliability of the results obtained by the standardless approach.

The investigation of the physical-chemical properties of micro sized particles presents both a considerable interest and a big challenge. Typical samples of interest are powders of uranium compounds used in the nuclear industry and uranium particles mixed with environmental and industrial dust (referred to as "environmental samples" taken by IAEA's inspectors in nuclear facilities). Most of these samples are composed of microparticles that exhibit an irregular and complex morphology with heterogeneous compositions, sizes and morphologies. Geometrical and elemental characterization of each particle individually are generally required.

In many years, spectroscopy techniques showed a great use in investigating both the composition and morphology of individual particles. Electron probe microanalysis (EPMA) is among the techniques enabling to analyze solid samples in a microscopic volume which gives the possibility to perform both qualitative and quantitative analysis of microparticles. Complementary methods based on vibrational spectroscopy are also considered to be powerful for molecular characterization. In particular, micro-Raman spectrometry (MRS) offers a better special resolution of 1-10 µm than other techniques such as micro-infrared spectroscopy, allowing the investigation of particles of few micrometers.

In EPMA, analysis based on standards is usually used to quantify the composition of samples with unknown stoichiometry. The methodology consists in comparing the X-ray intensities of the unknown sample to the intensities of a standard material, and uses conventional **ZAF** or $\varphi(\rho z)$ correction procedures to take matrix effects into account[1,2]. However, **ZAF** and $\varphi(\rho z)$ models were basically developed for bulk polished specimens and cannot be applied accurately to quantify the composition of powders made up of microparticle assemblies. This is mainly due to the difference between a micrometer sized particle and a bulk material in terms of absorption path lengths, electron interaction volume and fluorescence emission.

In order to deal with these limitations, standardless methods[3] can be applied, where X-ray intensities are calculated and used as virtual standards. Numerous works have shown promising results when the calculation of X-ray intensities is performed by Monte Carlo (MC) simulations[4,5,22]. It is presumed that by including instrument characteristics as well as the morphological and physical-chemical properties of samples, rigorous corrections can be obtained. MC simulations have also been proven to be viable to dealing with complex analysis in non-conventional samples such as microparticles[5] and thin films[7].

In MC codes, the interactions of electrons and photons with matter are described by a set of differential cross sections

(DCSs) that characterize the probability distribution of each interaction mechanism. Nevertheless, even the most accurate and widely used approaches for cross section determination are based on approximations, which may lead to multiple uncertainties. For instance, Campos et al. estimated uncertainties to be around 5% for K lines in the atomic number range $4 \leqslant Z \leqslant 40$, when ionization cross sections are obtained from a distorted-wave Born approximation based model[11]. While it is important to consider uncertainties in the case of L and M shells, their estimation is rather difficult. This is mainly due to the complexity encountered when determining atomic parameters such as fluorescence yields ω_i and Coster-Kronig (CK) transitions f_{ij} that are involved in the process of converting measured intensities into ionization cross sections. Approximate theoretical models such as the Dirac-Hartree-Slater (DHS) and Dirac-Fock (DF) models were developed and used to provide databases of atomic parameters[12,13]. The reliability of these parameters becomes of great importance when L and M lines are used in standardless procedures.

Standardless quantification of uranium samples is a typical example where M and L lines are used. Merlet et al. and Moy et al. showed that theoretical calculations of M-subshell X-ray production cross sections can be carried out with good accuracy using atomic parameters based on DHS and DF models[14,15]. These studies were performed on heavy elements, Au, Pb, Bi, U and Th. The authors compared the measured X-ray production cross sections for these heavy elements and those calculated from Bote et al.[10] ionization cross sections, and showed that the Bote et al. analytical model can be accurately used for standardless quantification[16].

In standardless analysis based on MC simulations, the geometry of the sample is also an important parameter that needs to be included in the simulation. Some MC codes such as PENELOPE[20] (Penetration and ENErgy LOss of Positrons and Electrons) and NISTMonte-DTSA-II[5] use geometrical packages that enable different geometries to be built. However, some particles have very complicated shapes that would take a tremendous time and effort to describe accurately. Moreover, particles often exhibit a surface roughness which adds more complexities in the construction of their geometry. Rough surfaces can be responsible for a loss in the measured X-ray intensities which might lead to multiple uncertainties if the surface texture is not integrated in simulations.

It has been demonstrated, that the loss of X-ray signal in EPMA due to surface roughness can be taken into account using a peak-to-background (P/B) method[19]. The assumption that the depth distributions of both characteristic and continuum radiations are similar, guarantees the independence of their ratio with respect to electron incidence angle and absorption path lengths. This accounts for the variation in the emission of X-rays caused by textural effects. P/B correction methods were used in a number of standardless approaches and provided good accuracy in the quantitative analysis[17,18].

Being almost independent of absorption, P/B ratios can also be used to compensate for the difference between X-rays emission inside a particle and inside a bulk material. Nevertheless, for very small particles where the X-ray depth range is larger than the size of the particle, the transmission of electrons through the particle takes place and influences significantly the calculated $\frac{P}{B}$ ratios[21]. In fact, the X-ray production cross section of characteristic and continuum radiations varies differently in terms of the X-ray generation depth[21,34] which results in P/B ratios strongly dependent of the thickness of the particle[17,21]. Transmitted electrons can also excite the substrate atoms if they exit the particle with sufficient energy. In this case, the substrate behaves like a secondary source of X-rays which interferes with the process of X-ray emission inside the particle.

These limitations make quantitative EPMA of microparticles complicated and challenging. Otherwise, the use of other characterization techniques in combination with EPMA enables to put more confidence in EPMA quantitative results. For instance, MRS was successfully applied to the molecular characterization of small sized aerosol particles[6]. The combined use of EPMA and MRS has been reported in another study[8]. MRS have also been proven to provide accurate results when applied to uranium particles[9,28]. Pointurier et al. showed that Raman bands of uranium compounds can be detected and distinguished in uranium airborne microparticles[9]. In the case of pure compounds, MRS allows determining the stoichiometric composition of micrometer-size particles and thus provides their elemental composition. Besides, it is worth considering that even if the analyzed particles come from a bulk material of known composition, the composition of micrometric particulate material extracted from the surface of the source material may have been modified by oxidization/reduction or hydration processes. In such cases, it is likely to observe some differences between the quantitative results obtained by EPMA and the expected composition of the studied particles. MRS is more sensitive to the changes due to surface oxidation and hydration, which may help explaining the observed differences with EPMA results.

In the present work, the ZAF peak-to-background quantitative procedure[17] was applied in combination with MC simulations to quantify spherical microparticles of K411 glass and uranium microparticles with irregular shapes. Simulated P/B ratios were obtained from the 2012 version of the general-purpose MC code PENELOPE[20], which uses Bote et al. ionization cross sections. After taking into account the spectrometer resolution function, the simulated P/B ratios were used in the quantitative procedure. Effects due to the transmission of electrons were accounted for by performing simulations on a particle with a thickness equal to the mean distance travelled by electrons before exiting the analyzed particle. We describe a simple model that allows to determine the mean distance that electrons travel in irregularly shaped uranium particles using the measured characteristic line of the substrate on which the particles are deposited. The chemical composition of uranium particles was further investigated by MRS and compared to the results obtained by the standardless approach.

The ZAF P/B standardless approach[17] was basically applied to quantify particles by using K and L lines. To our knowledge, the method has not yet been applied to quantifying particles of heavy elements such as uranium microparticles for which the use of M lines can be necessary.

EXPERIMENTAL AND SIMULATION

EPMA measurements. Measurements were performed using an Oxford energy dispersive spectrometer attached to a Merlin field-emission scanning electron microscope. The spectrometer positioned at a take-off angle of ~35° from the sample, is com-

posed of a silicon drift detector (SDD) and an AP3 Moxtek window supported by a rigid silicon grid. The distance between the spectrometer and the sample was set at 19.5 mm so as to collect a maximum number of emitted photons. The electron energy was set to 20 keV except for measurements of the apparent thicknesses, where different electron energies were used.

All intensity measurements were performed using the longest shaping time so as to obtain a resolution of 125 eV FWHM at Mn Kα. The electron probe current was optimized in each case so that the counting rate do not exceed 30% in its dead time. Characteristic intensities were determined after subtracting the background from measured spectra, and normalizing the resulting number of counts at the top of the peak by the number of primary electrons. Uncertainties associated to counting statistics were within 1-3% for characteristic lines and about 4-8% for continuum radiations. The precision in determining the number of incident electrons was estimated to be about 2% using a Faraday-cup.

Monte Carlo simulations. Simulated X-ray intensities are given in absolute units, as the probability of collecting one photon per unit solid angle, per incident electron, and per unit photon energy. PENELOPE uses an ideal detector to collect the emitted photons. Although P/B ratios are independent of instrumental parameters, they are a function of the energy resolution. Therefore in order to obtain simulated P/B ratios that could be compared to the measured ones, the detector resolution function was implemented in the code. PENELOPE enables with its subroutine package "CONVOLG" to integrate the resolution function of the detector.

Since simulated spectra in absolute units do not contain any spectral broadening, theoretical Bremsstrahlung intensities are simply determined from the mean value of the two intensities on each side of the characteristic line of interest. The reliability of the Bremsstrahlung simulation given by PENELOPE has already been demonstrated in previous studies[4,24].

For the sake of accuracy and time optimization, a hemispherical detector was used in the simulation to work with a large collection zone of emerging photons. The simulations were thus limited to cases where the electron beam strikes at normal incidence so as to obtain a symmetrical X-ray distribution function inside the particle. Even if this configuration do not adhere to how real measurements are performed, the use of P/B ratios allows to a reasonable degree to compensate for the differences in the X-ray emission caused by both the difference in absorption path lengths and the incidence angle of the electron beam.

Correction of transmission effects. In microparticles smaller than the X-ray generation range, transmission effects were accounted for by performing simulations on a particle with a thickness equal to the mean distance that electrons travel before crossing the analyzed particle. For particles with irregular shapes, this distance was determined from the intensity P_s corresponding to the K line of the substrate on which the particle is deposited. We will assume that the characteristic X-ray intensity emitted from the substrate is mainly influenced by i) absorption inside both the substrate and the particle, ii) backscattering effects from the surface of both the particle and the substrate and iii) the energy of electrons after crossing the particle. By using the equation of Green and Cosslett [25] for characteristic intensities, we can write:

$$P_s \approx f(\chi_s, E_0') f\left(\chi_p, E_0\right) R_s(E_0') R_p(E_0) \frac{E_0' \ln \frac{E_0'}{E} - E_0' + E}{E} \quad (1)$$

where χ_p, χ_s are respectively the mass absorption coefficients inside the particle and the substrate, E (keV) the photon energy corresponding to the K line of the substrate element, E_0 (keV) is the energy of incident electrons and E_0' (keV) is the energy of electrons that are transmitted through the particle. $f(\chi_s, E_0')$, $f\left(\chi_p, E_0\right)$, $R_s(E_0')$ and $R_p(E_0)$ are absorption and backscattering factors of the substrate and the particle respectively. E_0' can be expressed in terms of E_0 as[23]:

$$E_0' = E_0\left(1 - \frac{S}{Y}\right)^{3/5} \quad (2)$$

where S (μm) is the distance travelled by electrons after crossing the particle and Y (μm) the Kanaya-Okayama (K-O) electron range radius[23] expressed as:

$$Y = \frac{0.0276\, A\, {E_0}^{1.67}}{Z^{0.89}\, \rho} \quad (3)$$

with A the atomic mass (g), Z the atomic number and ρ the density (g cm^{-3}). The X-ray spectra of the particle were later measured at different energies of incident electrons E_{0_j} (j=1,2...m) and the characteristic X-ray intensity corresponding to the K line of the substrate was determined in each case. For the sake of precision, the value of m was set equal to 7. The characteristic intensities emitted from the substrate are afterward normalized by the intensity obtained at one of the electron energies e.g. the highest one E_{0_m}. This enables, to a reasonable degree, eliminating the dependence on the absorption inside the particle. Now, if we neglect the variation of the backscattering factors in terms of electron energy, which is a reasonable consideration in a small energy range[33], we can express the normalized intensities as:

$$\frac{P_s(E_0)}{P_s(E_{0_m})} = \frac{f(\chi, E_0')_s}{f(\chi, E_{0_m}')_s} \frac{\left(1 - \frac{Q}{{E_0}^{1.67}}\right)^{\frac{3}{5}}}{\left(1 - \frac{Q}{{E_{0_m}}^{1.67}}\right)^{\frac{3}{5}}} \times \frac{\left(E_0 \ln\left(\frac{E_0\left(1 - \frac{Q}{{E_0}^{1.67}}\right)^{\frac{3}{5}}}{E}\right) - E_0 + \frac{E}{\left(1 - \frac{Q}{{E_0}^{1.67}}\right)^{\frac{3}{5}}}\right)}{\left(E_{0_m} ln\left(\frac{E_{0_m}\left(1 - \frac{Q}{{E_{0_n}}^{1.67}}\right)^{\frac{3}{5}}}{E}\right) - E_{0_m} + \frac{E}{\left(1 - \frac{Q}{{E_{0_m}}^{1.67}}\right)^{\frac{3}{5}}}\right)} \quad (4)$$

with

$$Q = \frac{S\, Z^{0.89} \rho}{0.0276\, A} \qquad (5)$$

The normalized intensities as a function of E_0, are afterward fitted by equation (4) with Q the parameter to fit. On the other hand, the K-O X-ray depth range can be expressed as:

$$Y_{Xr} = \frac{0.0276\, A\, ({E_0}^{1.67} - E^{1.67})}{Z^{0.89}\, \rho} \qquad (6)$$

We can write:

$$\frac{\rho\, S}{\rho Y_{Xr}} = \frac{Q}{{E_0}^{1.67} - E^{1.67}} \qquad (7)$$

By replacing ρY_{Xr} with an expression similar to the one given by Anderson and Hasler[31], the distance S in µm can be determined by:

$$S = \frac{Q}{\rho\, ({E_0}^{1.67} - E^{1.67})}\; F\, ({E_0}^{1.68} - E^{1.68}) \qquad (8)$$

F is a constant that was set equal to 0.064 in Anderson and Hasler's formula. A better description was given by Hovington[36] where F was expressed in terms of the atomic number Z. In this work F was adjusted over a wide range of atomic numbers in order to reasonably predict the values of the K-O X-ray depth range. A value of F = 0.068 was found for $6 \leq Z \leq 12$, 0.075 for $13 \leq Z \leq 29$, 0.096 for $30 \leq Z \leq 71$ and 0.112 for $Z > 71$. We will refer to the distance S as the apparent thickness (t_{app}) of the particle so as to make a distinction between the distance that electrons travel before crossing the particle and the true thickness of the particle.

Standardless quantitative EPMA. The quantitative procedure adopted in this work was based on the Lábár and Török P/B model[17] where the concentration of the *i*th element in the unknown sample is determined using the following corrected ZAF approach:

$$C_i = k_i\, Z_c\, R_c\, A_c\, F_c \qquad (9)$$

with Z_c, R_c, A_c and F_c are respectively factors for the correction of atomic number, backscattering, absorption and fluorescence. k_i is the k-ratio of the P/B for the *i*th element in the unknown sample to the one in the standard:

$$k_i = \frac{(P/B)^{unknown\ sample}}{(P/B)^{standard}} \qquad (10)$$

According to the authors the main influence is due to atomic number effects and R_c, A_c and F_c are second order corrections. The atomic number is corrected using the ratio $Z_c = (Z_{mean}/Z)^{0.00599E_0+1.05}$, with Z_{mean} the mean atomic number of the sample and Z the atomic number of the element in question. In this work, simulated P/B ratios were used in equation (10) and enabled to determine weight fractions from the following expression:

$$C_i = \frac{(P/B)^{unknown\ sample}}{(P/B)^{simulated}}\, Z_c\, R_c\, A_c\, F_c \qquad (11)$$

In order to correct for transmission effects and substrate parasitic signals, a configuration where the particle is deposited on a flat substrate was constructed. The construction was performed using the PENGEOM geometry package of PENELOPE. The method used in PENGEOM is based on meshing homogeneous primitive bodies with conventional shapes limited by quadric surfaces.

Bremsstrahlung intensities used in experimental $\frac{P}{B}$ ratios were determined *a priori* by constructing the background of each measured spectrum. Characteristic escape and pile-up peaks were removed from the measured X-ray spectrum and detection efficiency corrections were carried out using the method of Merlet et al.[24]. If we suppose that the measured continuum spectrum of a particle deposited on a substrate is a sum of the particle and the substrate backgrounds (B_p and B_s respectively) the measured background B_{total} can be fitted using the following model:

$$B_{total}(E) = B_p(E) + B_s(E) \qquad (12)$$

that can be written as[29]:

$$B_{total}(E) = K\, f(\chi_p, E_0) \left[\left({Z_p}^n \left(\frac{(E_0 - E)}{E} \right)^n \exp(B) \right) + f\left(\chi_s, E_0^{'}\right) {Z_s}^{n'} \left(\frac{\left(E_0^{'} - E\right)}{E} \right)^{n'} \exp\left(B^{'}\right) \right] \qquad (13)$$

where K is a scaling factor, $n = 0.00599E_0 + 1.05$, $B = -0.0322E_0$, B' and n' are calculated at E_0'. Now, by using Love and Scott[33] absorption factor along with the expression given by Thinh and Leroux for mass absorption coefficients[32], we can write:

$$B_{total}(E) = K \frac{\left(1 - \exp\left(-2\, h \left(\frac{12.4}{E}\right)^l\right)\right)}{2h\left(\frac{12.4}{E}\right)^l} \left[\left({Z_p}^n \left(\frac{(E_0 - E)}{E} \right)^n \exp(B) \right) + {Z_s}^{n'} \left(\frac{\left(E_0^{'} - E\right)}{E} \right)^{n'} \exp\left(B^{'}\right) \frac{\left(1 - \exp\left(-2\, r \left(\frac{12.4}{E}\right)^x\right)\right)}{2\, r \left(\frac{12.4}{E}\right)^x} \right] \qquad (14)$$

where K, h, Z_p, l are parameters to fit, r and x are determined *a priori* from fitting mass absorption coefficients corresponding to the elements composing the substrate. Since mass absorption coefficients are presented as a continuous function, it is recommended to perform the fitting at separate energy intervals so as to reduce inaccuracies associated to absorption edges. For particles that are not affected by transmission effects, the background associated to the substrate should be extracted from the fitting model. It is worth noting that even though equation (14) enables to perform a simple and satisfactory construction, it

does not account for the loss due to electrons backscattering. This could have significant effects if the substrate is composed of heavy elements. The model will be refined in future studies to integrate backscattering factors. Having a more precise model might be useful if seeking to predict unknown parameters such as the mean atomic number of the particle or, in the best cases, to determine and remove the parasitic contribution of the substrate from the total measured background.

Analysis with micro-Raman spectrometry. Analyses of uranium particles were carried out with a Renishaw 'In Via' MRS equipped with two laser wavelengths, 785 nm and 514 nm with maximum powers of 300 and 50 mW respectively. This instrument is coupled to a SEM (FEI XL-30) equipped with an EDX analyzer, so that Raman analysis is carried out within the SEM measurement chamber[37]. This coupling allows obtaining electronic images, elemental composition and molecular composition for the same micrometric spot. In this study, 'Wire' software package provided with the MRS was used to process the spectra with the following method: i) correction of the baseline of each spectrum by manually selecting points across the baseline and using cubic spline interpolation; ii) application of an iterative curve fitting procedure to each spectrum, after initial approximate identification by the user of the position, height and width of the Raman bands. Analyzed area are ~1 µm^2 and ~4 µm^2 with the 514 nm and 785 nm lasers, respectively. Raman spectra were acquired with both lasers for each uranium particle. Spectral range was 150—1400 cm^{-1}. Incident laser powers were typically ~0.5 mW for both lasers and acquisition times were 300 seconds (5×60 s).

RESULTS AND DISCUSSIONS

Individual spherical K411 microparticles. In order to validate the reliability of the quantitative approach based on equation (11), X-ray measurements were made on NIST homogeneous spherical particles of K411 glass. When probing particles that have a size smaller than the electron depth range, transmission of electrons occurs. Transmitted electrons do not contribute in the X-ray generation process and can be responsible for a loss in the X-ray signal in a similar way as if they are backscattered. Transmitted electrons can also excite the substrate atoms which results in a parasitic X-ray emission. The substrate is regarded in that case as a source of radiation that contributes in the total measured background and might also cause a secondary fluorescence emission inside the particle.

Simulations were therefore performed on a similar configuration as the real one i.e. a spherical particle on a flat substrate. Weight fractions were determined using equation (11) for 0.6 and a 0.8 µm K411 glass particles both deposited on a nickel substrate. We show in Table 1 calculated weight concentrations Cc obtained from equation (11) in comparison with nominal concentrations Cn.

It can be concluded that the calculated concentrations are in good agreements with the certified ones with deviations that do not exceed 9% in absolute values. This enables to validate the accuracy of equation (11) and the methods used to determine the experimental and simulated P/B ratios. It must be noted that discrepancies in the determination of experimental Bremsstrahlung intensities can lead to significant deviations in the calculated concentrations. Great attention should therefore be given to the model used for the construction of the measured background.

Table 1. Average quantitative results Cc obtained from equation (11) for K411 spherical particles and their corresponding expanded standard uncertainties (coverage factor k=2). The composition of the particles is certified by the National Institute of Standards and Technology as Cn%(O)=42.9±1.2, Cn%(Mg)=9.2±1.4, Cn%(Si)=25.6±1.7, Cn%(Ca)=11.2±2.3 and Cn%(Fe)=11.2±2.3. $Dev\,\% = \frac{Cc-Cn}{Cn} \times 100$ represents the deviation from nominal concentration Cn.

	Cc %(0.6µm)	Dev (%)	Cc %(0.8µm)	Dev (%)
O	41.3±1.5	-3.7	42.5±1.2	-0.9
Mg	9.7±0.5	+5.4	9.3±0.7	+1.0
Si	26.7±1.2	+4.3	24.1±1.4	-5.9
Ca	10.9±0.8	-3.6	11.8±0.8	+2.6
Fe	11.3±0.9	+0.9	12.2±0.7	+8.9

An accurate quantitative analysis of micro sized particles can only be obtained if the loss in the X-ray signal caused by the transmission of electrons is corrected. Generally, the thickness of the studied microparticle can give an idea about the apparent thickness i.e. the distance travelled by transmitted electrons inside the particle. However, for particles that have an irregular shape, it is very complicated to accurately estimate the apparent thickness. Moreover, the transmission of electrons is related to scattering path lengths of electrons before crossing the particle and correcting for transmission effects by using the apparent thickness is more reasonable than using the true thickness of the particle.

On the other hand, electrons that exit the particle induce an X-ray emission from the substrate. The X-ray intensity emitted from the substrate can be used as a good indicator of the apparent thickness of the particle. The emission of the substrate can also allow to determine the true thickness if the studied particle is sufficiently compact. The method used for the determination of the apparent thickness was tested on three K411 homogeneous spherical microparticles a), b) and c) of different sizes deposited on an aluminum substrate. We present in Table 2 the diameter of the spherical particles as well as the apparent thickness calculated using equation (8).

Table 2. Apparent thicknesses "t_{app}" determined for three NIST spherical particles of K411 glass.

	Diameter of the particle	t_{app}
a)	0.84 µm	0.73 µm
b)	2.03 µm	1.97 µm
c)	3.03 µm	2.94 µm

It can be seen that the values of the apparent thickness S determined from equation (8) are in satisfactory agreements with the true thickness of the particles. Generally, the calculated apparent thickness is slightly smaller than the diameter of the spherical particles. This probably results from the fact that some electrons exit the particle through side scattering with an energy higher than if they are transmitted at a depth equal to the diameter. These side scattered electrons increase the mean energy E_0' of transmitted electrons that reach the substrate which leads to an estimated thickness lower than the diameter. Nonetheless, if one's aim is to determine the true thickness of the particle with

more precision, it is possible to refine the calculations by using high energies of incident electrons E_0. This enables to reduce the amount of side scattered electrons and obtain trajectory segments of electrons that are more parallel.

Uranium microparticles. The analysis was further applied on uranium microparticles with irregular shapes deposited on an aluminum substrate for EPMA analysis and on sticky carbon surfaces mounted on aluminum tapes for MRS analysis. EPMA and MRS analyses were not carried out on the same particles. Three groups of particles were studied separately in terms of their expected chemical composition: group 1 of uranium tetrafluoride (UF_4), group 2 of triuranium octoxide (U_3O_8) and group 3 of uranium dioxide (UO_2). Particles with irregular shapes often exhibit a variable thickness and correcting for transmission effects in EPMA using an estimated constant thickness can lead to wrong results. Therefore, the loss due to the transmission of electrons can only be corrected accurately if the thickness is determined at a specific incidence point of electrons. In this study, the analysis was performed at randomly chosen incidence points of a focused electron beam for which a corresponding apparent thickness was determined and used in simulations. MRS was later used as a complementary technique to investigate the composition of 10 to 12 uranium microparticles of each group.

***Group 1*.** Particles of group 1 exhibited an irregular shape with a variable thickness. The apparent thickness was determined for four randomly selected particles (Part 1, 2, 3 and 4), by measuring the X-ray spectra at an electron incidence point represented by the red circle in figure 1. We present in figure 2 the X-ray spectrum measured for each particle as well as the determined apparent thicknesses (t_{app}).

As expected the emission of the substrate is more important for the particle "Part 2" that has the lowest apparent thickness. We can observe an intensity loss in the particle "Part 3" for both characteristic and Bremsstrahlung intensities especially at low photon energies. This was attributed to textural effects since the incidence point of the focused electron beam is located at a zone where the particle exhibits a high surface roughness. In quantitative analysis, the intensity loss due to textural effects can lead to significant errors in the calculated concentrations. Using $\frac{P}{B}$ ratios enables, to a reasonable degree, compensating for this loss[19], thus, a P/B quantitative approach appears to be very suitable in dealing with microparticles exhibiting surface roughness.

The apparent thicknesses were later used in simulations to correct for transmission effects. The concentrations were calculated (see Table 3) for each particle and showed a chemical composition close to an UF_4 compound, although F concentrations are slightly overestimated (on average an excess of 3%) with respect to expected concentration in UF_4.

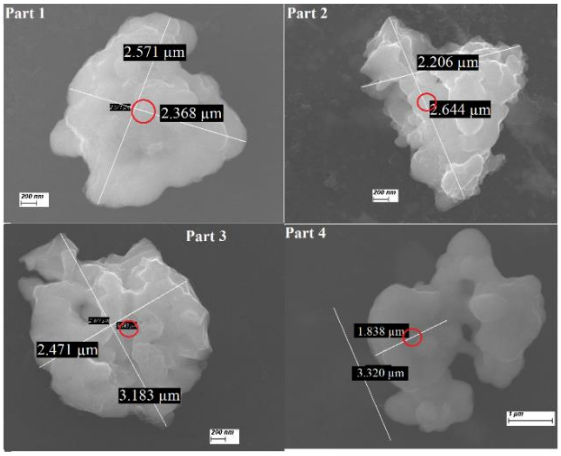

Figure 1. SEM images of uranium particles of group 1.

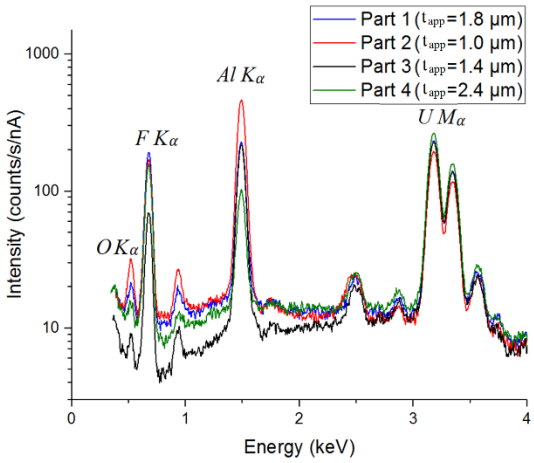

Figure 2. X-ray spectra of uranium particles of group 1 at an electron energy of 20 keV. The measurements were performed using a focused electron beam at an incidence point represented by the red circle in figure 1.

Table 3. Average quantitative results Cc obtained from equation (11) for uranium particles of group 1 and their corresponding expanded standard uncertainties (k=2). "t_{app}" represents the apparent thickness determined for each particle.

	t_{app} (µm)	Cc %(U)	Cc %(F)
UF_4	-	75.8	24.2
Part 1	1.8	71.3±1.0	28.7±1.0
Part 2	1.0	71.6±1.2	28.4±1.2
Part 3	1.4	73.1±1.4	26.9±1.4
Part 4	2.4	74.8±0.7	25.1±0.7

MRS was further applied to investigate the composition of particles of group 1. Three different Raman spectra associated to three different uranium compounds (figure 3) were observed. All Raman spectra exhibit a more or less intense very broad fluorescence peaks centered at ~900 cm^{-1} with the 514 nm laser and ~300 cm^{-1} with the 785 nm laser, which is a characteristic spectral feature of UF_4 in Raman spectroscopy[9,38]. However, some of the spectra show a Raman band at 915 cm^{-1} (U-O elongation) indicating the presence of anhydrous uranium oxyfluorides[39] (UO_2F_2) or a band at 870 cm^{-1} (elongation of the uranyl ion UO_2^+) which is attributed to the presence of a hydrated UO_2F_2 [28,39]. This shows that the UF_4 particles underwent partial

oxidization/hydration with a loss of fluorine. The Raman spectrum acquired for other particles only showed the spectral feature of the UF_4 compound. It should be noted that the presence of oxygen can also be observed in the X-ray spectra (figure 2) with a very weak characteristic X-ray intensity. Since the analysis of MRS is performed at a depth much lower than in EPMA (likely no more than a few tens of nm), we expect that the oxygen signal observed in some particles originated from an oxidation layer of at most a few tens of nanometers on the surface. Whatever it may be, this partial surface oxidization/hydration of the particles, which results in a relative loss of fluorine, certainly does not explain the slight excess of F found by EPMA analysis. We currently have no explanation for this calculated excess.

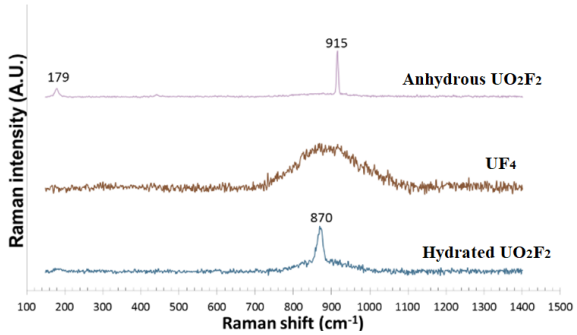

Figure 3. Typical examples of Raman spectra obtained for uranium particles of group 1 (514 nm laser).

***Group 2*.** Three particles of group 2 (Part 5, 6 and 7) were randomly chosen for analysis with EPMA. As illustrated in figure 4, X-ray measurements showed an important presence of both oxygen and uranium. A significant emission of the aluminum substrate resulting from the transmission of electrons was also observed. Transmission effects were further corrected after determining the apparent thickness for each particle. We illustrate in table 4 the quantitative results obtained for the three particles showing a composition of an U_3O_8 compound.

Analysis were afterward, performed with MRS. The Raman spectrum presented in figure 5 was repeatedly obtained for almost all the particles and shows Raman bands at 347, 418 and 808 cm^{-1} characteristic of U-O stretching and a band at 738 cm^{-1} characteristic of O-U-O-U stretching. These observations indicate the presence of an U_3O_8 compound[9,40] which agrees with the quantitative results given by the standardless approach.

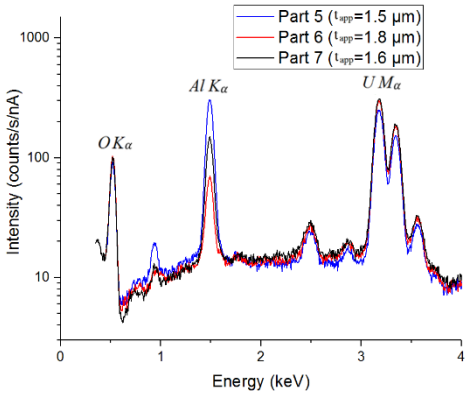

Figure 4. X-ray spectra of uranium particles of group 2 measured at electron energy of 20 keV.

Table 4. Average quantitative results Cc obtained from equation (11) for uranium particles of group 2 particles and their corresponding expanded standard uncertainties (k=2). "t_{app}" represents the apparent thickness determined for each particle.

	t_{app} (µm)	Cc %(U)	Cc %(O)
U_3O_8	-	84.8	15.2
Part 5	1.5	84.6±0.9	15.4±0.9
Part 6	1.8	84.2±0.7	15.8±0.7
Part 7	1.6	83.7±1.2	16.3±1.2

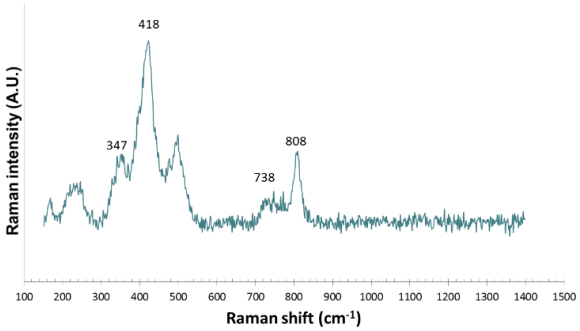

Figure 5. Typical Raman spectrum obtained for almost all the studied uranium particles of group 2 (514 nm laser).

***Group 3*.** Particles of group 3 exhibited an agglomerated form with high surface roughness. Two particles were selected and studied and both were affected by transmission effects. Figure 6 shows SEM images of the two particles (figure 6a), the incidence point of the focused electron beam (figure 6a) and the X-ray spectrum measured at each incidence of the electron beam (figure 6b).

The X-ray spectra show the presence of oxygen and uranium as well as a characteristic peak of the aluminum substrate. The apparent thickness determined for the particle "Part 8" of 0.7 µm explains to some degree the important substrate emission observed in its corresponding X-ray spectrum. Table 5 illustrates the quantitative results obtained for the two particles.

It can be observed that the calculated concentrations indicate an amount of oxygen slightly higher than in an UO_2 compound. Analysis with the 785 nm laser of the MRS performed on particles of group 3 showed two Raman bands at ~450 cm^{-1} and a more intense and broader band at ~620 cm^{-1} (figure 7, red spectrum). As shown by Desgranges et al.[41], the first band correspond to the reminiscent T_{2g} Raman stretch mode of UO_2 whereas the second observed band is characteristic of an U_4O_9 compound probably resulting from an oxidation in the surface of UO_2 particles. Analysis carried out with the 514 nm laser on the same particles (figure 7, blue spectrum) showed three bands at 445, 576 and 1150 cm^{-1}. As mentioned above, the peak at 448 cm^{-1} is the Raman T_{2g} band characteristic of UO_2. The observed band at 1150 cm^{-1} was attributed to light scattering from phonons as a result of the collective vibrations of the crystalline lattice (2 L-O phonon), which is observable with the 514 nm laser, but not with the 785 nm one. The peak at 576 cm^{-1} is not observed in pure stoichiometric UO_2. However, as the UO_2 structure is distorted into U_4O_9, the point symmetry in UO_2 structure is lowered, so that the 1-LO mode at 575 cm^{-1} which

is Raman-forbidden in UO_2 is allowed in U_4O_9[41]. It should be noted that the broad band at ~620 cm^{-1} assigned to U_4O_9 cannot be observed with the too low frequency 514 nm laser. So combination of MRS spectra with 514 nm and 785 nm lasers shows coexistence of UO_2 and U_4O_9 compounds in the analyzed volumes. Indeed, UO_2 is not thermodynamically stable in air and is readily oxidized, leading to an oxidation layer with a depth of a few ten of nm, depending on time spent and on the atmosphere[42]. Therefore, it is not surprising that UO_2 particles may contain a small fraction of U_4O_9. The results in Table 5 show an influence of the oxidation layer much important for "Part 8". This might be a consequence of the low apparent thickness of "Part 8" which results in a reduced X-ray generation volume in the core of the particle where UO_2 is mostly present.

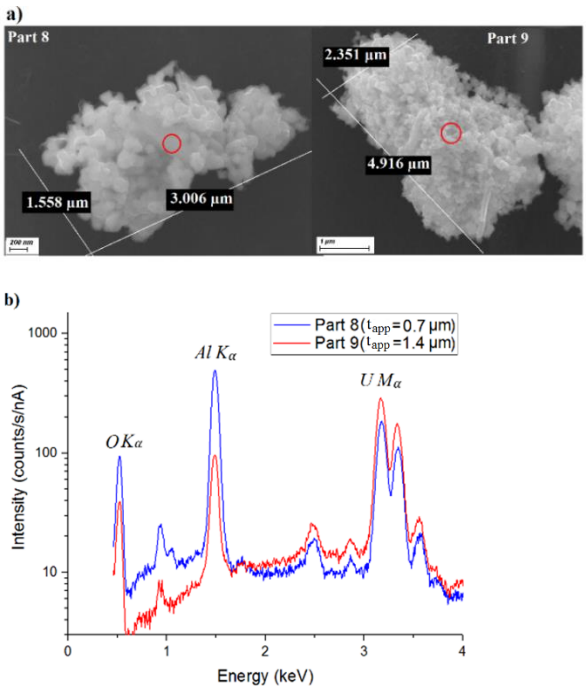

Figure 6. a) SEM images of uranium particles of group 3 and **b)** the X-ray spectra measured for each particle at electron energy of 20 keV.

Table 5. Average quantitative results Cc obtained from equation (11) for uranium particles of group 3 and their corresponding expanded standard uncertainties (k=2). "t_{app}" represents the apparent thickness determined for each particle.

	t_{app} (µm)	Cc %(U)	Cc %(O)
UO_2	-	88.1	11.9
Part 8	0.7	85.6±1.1	14.4±1.1
Part 9	1.4	87.1±0.7	12.9±0.7

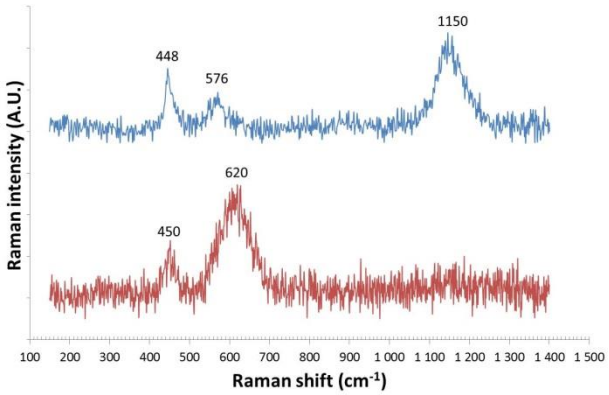

Figure 7. Typical Raman spectra observed for a set of uranium particles of group 3 (red spectrum: 785 nm laser, blue spectrum: 514 nm laser).

CONCLUSIONS

The chemical state of uranium microparticles with irregular shapes was investigated with the combined use of standardless EPMA and MRS. Correction for the intensity loss in EPMA due to size effects in microparticles was achieved using a MC standardless approach based on a ZAF peak-to-background method[17]. The X-ray intensity loss due to the transmission of electrons through small particles requires knowledge of the distance that electrons travel before crossing the particle. As this distance can be approximated using the particle thickness, this no longer applies when particles exhibit and irregular shape with a variable thickness. The method based on equation (8) enables to cope with such a difficulty by determining an apparent thickness corresponding to the region where the focused electron beam entered the particle. This thickness is calculated by means of the X-ray characteristic intensity emitted from the substrate on which the particle is deposited.

The standardless approach in EPMA provides promising results with relative deviations $\frac{|Cc-Cn|}{Cn}$ <9% for K411 glass particles and a chemical composition of uranium particles that agrees to a certain extent, with MRS results. Indeed, MRS shows that UF_4 particles undergo partial oxidization/hydration into UO_2F_2 and that UO_2 particles are partially oxidized into U_4O_9. As this help explaining in the case of UO_2 particles, the small deviation in EPMA results with respect to theoretical composition, more efforts should be made to investigate the deviations observed in the case of UF_4 particles.

MRS gives information about the chemical composition on depths certainly not exceeding few tens of nanometers with the wavelengths of the used lasers. Consequently, results of the MRS analyses may not be fully representative of the particle composition, especially if the composition in the core of the particle is different than in the surface. EPMA enables to characterize particles in a much important depth which enables to cope with this difficulty. EPMA is however less sensitive to surface oxidation and hydration which are often encountered when analyzing uranium particles. This makes the combined use of the two techniques very complementary for the elemental investigation of micro sized uranium particles. Powdered materials of other uranium compounds such as UO_3 and $(U,Ce)O_2$ that often suffer phase transitions and oxidation/hydration phenomena, are worth studying and will be analyzed in a further study.

Although MRS analyses were made on different particles than those analyzed with EPMA, we plan for the future to perform EPMA and MRS analysis on the same particles thanks to fiducial marks visible with both instruments (EPMA and the SEM into which in-SEM Raman analyses are carried out) and a relocation algorithm.

Corresponding Author

E-mail : mouad.essani@cea.fr

Notes

The authors declare no competing financial interest.

ACKNOWLEDGMENT

We acknowledge the financial support of the cross-Disciplinary Program on instrumentation and Detection of CEA, the French Alternative Energies and Atomic Energy Commission.

REFERENCES

(1)Philibert J. Metaux Corrosion 40 (1964), Publication Irsid No B51. J. Microscopie 10. 6, 889 (1967)
(2)Pouchou, J.L. Pichoir F, (1991) In: Heinrich, K.F.J. and Newbury, D.E., Eds., Electron Probe Quantification, Plenum Press, New York, 31-75
(3)Trincavelli, J. ; Limandri S & Bonetto R (2014). Spectrochim Acta, Part B, 101, 76−85
(4)Merlet C & Llovet X (2006). Microchim Acta 155, 199–204
(5)Ritchie, N.W.M (2010). Microsc. Microanal 16, 248-258
(6)Potgieter-Vermaak S. S. & Grieken R,V (2006). Appl. Spectrosc. 60 39-47
(7)Hu, Y & Pan,Y (2001). X-Ray Spectrom. 30: 110–115
(8)S Sobanska, H.J Hwang, M Choël, H.J Jung, H.J Eom, H.K Kim, J Barbillat, C.U Ro (2012). Anal. Chem, 84,7, 3145-3154
(9)Pointurier F, Marie O (2010). Spectrochim Acta Pat B, 65 797-804
(10)Bote D & Salvat F (2008). Phys. Rev. A 77, 042701
(11)Campos C S, Vasconcellos M A Z, Trincavelli J, Segui S (2007). J. Phys. B: At. Mol. Opt. Phys. 40 3835–3841.
(12)Puri S (2007). At. Data Nucl. Data Tables 93 730-741
(13)Chen M.H & Crasemann B (1984). Phys. Rev. A: At. Mol. Opt.Phys. 30 170-176
(14)Merlet C, Moy A, Llovet X & Dugne O (2014). Surf. Interface Anal 46, 1170-1173
(15)Moy A, Merlet C & Dugne O (2014).Chemical Physics 440 18-24
(16)Moy A, Merlet C, Dugne O (2015). Anal. Chem, 87, 7779-7786
(17)Lábár J, Török S (1992). X-Ray Spectrom. 21 183–190
(18)Heckel J, Jugelt P (1984). X-Ray Spectrom. 13 159–165
(19)Newburry D E (2004), Scanning vol. 26, 103-114
(20)Salvat F, Fernández-Varea J. M. Sempau J (2011) J. PENELOPE-2011: A Code System for Monte Carlo Simulation of Electron and Photon Transport; OECD/NEA Data Bank, Issy-les-Moulineaux, France,
(21)Newbury D.E, Heinrich K.F.J Myklebust R.L, Small J.A (1980) National bureau of standards Spec Pub. 533. P. 39.
(22)Hovington P, Drouin D, Gauvin R(1997) CASINO: a new Monte Carlo code in C language for electron beam interaction -part I: description of the program, Scanning 19 1–14
(23)Kanaya K & Okayama S (1972). J. Phys. D :Appl. Phys. 5 43.
(24)Merlet C, Llovet X, Salvat F (2008). Phys. Rev. A: At., Mol., Opt. Phys 78, 022704
(25)Green M, Cosslett V. E., (1961). Proc. Phys. Soc. 78, 1206
(26)Philibert J. & Pattee H, Cosslett V, Engström A (1963) (Eds.), X-Ray Optics and X-Ray Microanalysis, Third International Symposium, Stanford, Academic Press, New York, p. 379
(27)Statham, P. J. (1979) Proc., Annu. Conf., Microbeam Anal. Soc., 14, 247-253
(28)Kips R, Pidduck A.J, Houlton M.R, Leenaers A, Mace J.D, Marie O, Pointurier F, Stefaniak E.A, Taylor P.D.P, Van den Berghe S, Van Espen P, Grieken R.V, Wellum R (2009) Spectrochim Acta Part B 60 199-207
(29)Small J, Leigh S, Newbury D, Myklebust R, (1987) J. Appl. Phys. 61 459–469.
(30)Henke B L, Gullikson EM, and Davis JC (1993), At. Data Nucl. Data Tables 54, 181-342
(31)Anderson C.A. & Hasler M.F (1966). Extension of electron microprobe techniques to biochemistry by the use of long wavelength X-rays. In Proceedings of the Fourth International Conference on X-ray Optics and Microanalysis, Castaing, R., Deschamps, P. & Philibert, J. (Eds.), pp. 310–327. Paris: Hermann.
(32)Thinh T.P, Leroux J. (1979). X-ray Spectrom. Vol. 8, No. 2
(33)Love G, Scott V D (1978), J. Phys. D: Appl. Phys. 11 1369
(34)Trincavelli J, Grieken R,V (1994). X-ray Spectrom 23, 254-260
(35)Reed S J B (1975). X-ray Spectrom. 4, 14-17
(36)Hovington, P., Drouin, D., Gauvin, R. & Joy, D.C. (1997). Parameterization of the range of electrons at low energy using the CASINO Monte Carlo program. Microsc Microanal 3(suppl. 2) 885–886
(37) Pointurier F., Marie O. (2013) J. Raman Spectrosc. 44, 1753-1759.
(38)Pidduck A.J., Houlton M.R., Williams G.M., Donohue D.L. (2008) IAEA-CN-148/115, Proceedings of the Symposium on International Safeguards, Vienna, Austria, 16–20 October 2008, 781–789.
(39)Armstrong D.P., Jarabek R.J., Fletcher W.H. (1989) Appl. Spectrosc. 43, 461-468.
(40)Allen G.C., Butler I.S., Anh Tuan N. (1987) J. Nucl. Mat. 144, 17-19.
(41)Desgranges L., Baldinozzi G., Simon P., Guimbretière G., Canizarès A. (2012) J. Raman Spectrosc. 43, 455-458.
(42)McEachern R.J., Taylor P. (1998) J. Nucl. Mater. 254, 87.